Applied Physics
Express

LETTER • **OPEN ACCESS**

Terahertz emission from intrinsic Josephson junctions in trilayer cuprate superconductor $Bi_2Sr_2Ca_2Cu_3O_{10+\delta}$

To cite this article: Manabu Tsujimoto *et al* 2025 *Appl. Phys. Express* **18** 073001

OPEN ACCESS

Applied Physics Express 18, 073001 (2025) LETTER

https://doi.org/10.35848/1882-0786/adda8e

Terahertz emission from intrinsic Josephson junctions in trilayer cuprate superconductor $Bi_2Sr_2Ca_2Cu_3O_{10+\delta}$

Manabu Tsujimoto[1*], Yifan Wen[2], Yoshiho Maeda[2], Asem Elarabi[3], Yilmaz Simsek[4], Ulrich Welp[5], Wai-Kwong Kwok[5], Shintaro Adachi[6], Takao Watanabe[7], and Itsuhiro Kakeya[2]

[1]Core Electronics Technology Research Institute, National Institute of Advanced Industrial Science and Technology (AIST), Tsukuba, Ibaraki 305-8565, Japan
[2]Department of Electronic Science and Engineering, Kyoto University, Kyoto 615-8510, Japan
[3]Quantum Dynamics Unit, Okinawa Institute of Science and Technology, Okinawa 904-0495, Japan
[4]Sabanci University Nanotechnology Research and Application Center, Tuzla, Istanbul 34956, Turkey
[5]Materials Science Division, Argonne National Laboratory, Lemont, IL 60439, United States of America
[6]Department of Mechanical and Electrical Systems Engineering, Kyoto University of Advanced Science (KUAS), Kyoto 615-8577, Japan
[7]Graduate School of Science and Technology, Hirosaki University, Hirosaki, Aomori 036-8561, Japan

*E-mail: m.tsujimoto@aist.go.jp

Received March 23, 2025; revised May 10, 2025; accepted May 18, 2025; published online July 17, 2025

This study presents the first observation of a continuous electromagnetic terahertz wave emission from mesoscopic mesas of the trilayer high-T_c superconductor, $Bi_2Sr_2Ca_2Cu_3O_{10+\delta}$ (Bi-2223), a putative Josephson plasma emitter utilizing intrinsic Josephson junctions. Two types of Bi-2223 crystals, optimally doped and underdoped, were prepared via thermal annealing under controlled partial oxygen pressures, and their electrical and emission characteristics were compared. A weak, but detectable terahertz emission was observed from the underdoped Bi-2223 mesas, whereas no radiation was observed from the optimally doped ones. We associate the low terahertz emission output with the weak capacitive coupling between the intrinsic junctions in the trilayer system. © 2025 The Author(s). Published on behalf of The Japan Society of Applied Physics by IOP Publishing Ltd

Electromagnetic waves in the terahertz frequency band hold great promise for various applications, such as cancer diagnosis, high-speed wireless communications, security and defense, and nondestructive imaging.[1–3] However, the development of terahertz technology has been impeded by the technical challenges involved in realizing solid-state terahertz sources within the frequency range of 0.5–1.5 THz. While powerful quantum cascade lasers have been developed for frequency bands above 1.5 THz;[4,5] however, these devices must be cooled to cryogenic temperatures and subjected to magnetic fields of several tesla.[6,7] On the low-frequency side, resonant tunnel diode oscillators show promise as room temperature terahertz sources, with maximum power levels of approximately 0.7 mW at frequencies of approximately 1 THz.[8]

Superconducting Josephson plasma emitters (JPEs) out of bulk single crystals of cuprate high-T_c superconductors have garnered considerable attention.[9–11] The JPE is based on Josephson oscillations in intrinsic Josephson junctions (IJJs), which exist naturally in single crystals of Bi-Sr-Ca-Cu-O (BSCCO) cuprates.[12] The IJJs comprise alternating atomic-scale stacks of superconducting Cu-O layers and Bi-O block layers. In the resistive state, the gauge-invariant phase difference changes over time, producing a high-frequency current that oscillates at the Josephson frequency $f_J = 2\,\mathrm{eV\,hN^{-1}}$, where e is the electronic charge, h is Planck's constant, and N is the number of resistive IJJs. Previous studies have reported broad emission frequencies in the tunable range from 0.15 to 2.4 THz[13–15] and detection of up to 11 THz emission from small-but-high mesa structures.[16,17] Coherent radiation up to 0.6 mW has also been achieved by synchronizing three mesas via Josephson plasma waves propagating through a BSCCO base crystal.[18,19]

Higher emission outputs and operating temperatures are desirable to improve the practical performance of JPEs. Recent studies on BSCCO have reported JPE operation above liquid-nitrogen temperature,[20–23] frequency control by altering the mesa structure acting as a cavity resonator,[24–26] and doping with different elements, such as lead (Pb) to heighten emission frequency.[27] However, device characteristics just below T_c are limited by material-specific superconducting properties, such as critical current and magnetic field penetration depth.

The BSCCO has a general formula of $Bi_2Sr_2Ca_{n-1}Cu_nO_{2n+4}$, and it has three different types: Bi-2201, Bi-2212, and Bi-2223, depending on the number of Cu-O planes per unit cell, n.[28] The T_c of BSCCO increases with n, e.g., Bi-2223 exhibits the highest T_c ~110 K. Moreover, the anisotropy of superconducting properties shows significant changes with n, making the mechanism of layered high-T_c superconductivity an attractive research topic in the field of superconducting devices. Especially, the presence of three CuO layers in the stack of Bi-2223 has attracted a great deal of interests because of its undefined role in the intrinsic Josephson junction effects. Although previous studies on JPEs have primarily focused on Bi-2212 driven by the availability of millimeter-sized single crystals, no studies have been reported using trilayer Bi-2223. The growth of large and pure Bi-2223 single crystals without Pb substitution remains challenging. Only a few research groups have reported the successful growth of large and pure Bi-2223 single crystals.[29–32] The stacks of IJJs in Bi-2223 single crystals provide not only a starting point to develop new JPEs operating above 100 K, but also insights into their synchronous behavior of thousands of stacked IJJs in a resonant mode. In the trilayer system, it has been proposed that the proximity between the underdoped inner plane with large pairing strength and overdoped outer plane with strong phase stiffness creates an optimal condition for superconductivity.[33–35] Josephson tunneling of Cooper pairs between inequivalent Cu-O planes within a unit cell has also been proposed as crucial for enhancing T_c.[36] Spectroscopic images from scanning tunneling

microscopy measurements revealed the absence of quasiparticle interference in the antinodal region of the overdoped samples, showing an opposite trend to that of single- and double-layer compounds.[37)]

In this study, we observed a terahertz emission from submillimeter-sized mesa structures fabricated using trilayer Bi-2223 single crystals with minimal defects, impurities, and inhomogeneities. The optimally doped Bi-2223 phase exhibits a maximum T_c of up to 109 K. We found that the power output emitted from the Bi-2223 IJJ stacks was significantly weaker than that of Bi-2212, which underlined the unique characteristics of Bi-2223 with its low capacitive coupling determined by the thickness of the superconducting Cu-O layers. These findings suggest that the macroscopic phase locking of the IJJ stack responsible for terahertz emission is significantly influenced by short-range capacitive coupling between adjacent IJJs.

The Bi-2223 single crystals were grown using the traveling solvent floating-zone method in an infrared mirror furnace. Our previous work describes the methodology in greater detail.[38)] Feed rods were synthesized by mixing Bi_2O_3, $SrCO_3$, $CaCO_3$, and CuO (with a purity greater than 3 N) to achieve the nominal composition $Bi_{2.25}Sr_{2.0}Ca_{2.0}Cu_{3.0}O_{10+\delta}$. The single crystals were grown at a rate of 0.05 mm h^{-1}, and the other growth conditions were identical to those used in our previous study.[38)] To adjust the excess oxygen amount, δ, we annealed crystals in a partial pressure-controlled oxygen atmosphere. In this study, two annealing conditions were used in the fabrication of the JPEs; optimally doped (OpD) and underdoped (UD). The OpD and UD crystals were annealed at 500 °C in 100% oxygen and 600 °C in 0.01% oxygen, respectively.

Table I summarizes the annealing conditions and related superconducting properties. The T_{conset} value is defined as the temperature at which the resistivity decreases because of the superconducting transition observed in c-axis resistivity measurements. The T_{conset} of 109 K for OpD agrees with the maximum value previously reported for the Bi-2223 phase.[33–35)] We determined the c-axis superconducting critical current J_c as the maximum switch current of the first quasiparticle branch at 35 K, where the transition from the zero-voltage state to the finite-voltage state occurred in c-axis current–voltage characteristic measurements.

Figure 1(a) depicts a high-resolution transmission electron microscope (HRTEM) image of as-grown Bi-2223 single crystals with slightly different chemical compositions from those used in this study, captured with the incident beam parallel to the b-axis direction (adapted from Ref. 39). In the HRTEM image, intergrowth Bi-2212 layers, constituting less than 2% of the bulk crystal, appear as dark lamellae, as indicated by the arrows. Although the atomic-scale microstructure shown in Fig. 1(a) varies slightly among different parts of the crystal batch, the results demonstrate that intergrowth Bi-2212 is present at a few percent under the current growth conditions. Figure 1(b) illustrates the temperature dependence of magnetic susceptibility, $\chi(T)$, for OpD Bi-2223 single crystal. The black and red plots represent field-cooled (FC) and zero-field-cooled (ZFC) $\chi(T)$ data, respectively. These data exhibit a singular and sharp superconducting transition with an onset temperature of 109 K, affirming the high quality of the single crystal. The presented data have been extracted and replotted from Ref. 38.

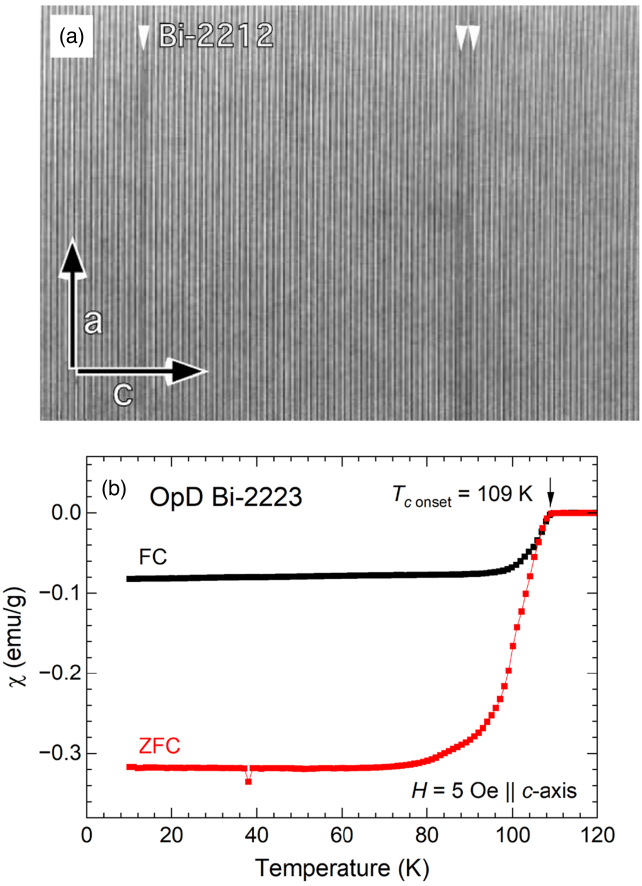

Fig. 1. (a) HRTEM image of as-grown Bi-2223 taken with the incident beam parallel to the b-axis direction (adapted from Ref. 39). Intergrowth Bi-2212 layers, constituting less than 2% of the bulk crystal, are visible as dark lamellae and are indicated by the arrows. (b) Temperature dependence of magnetic susceptibility, $\chi(T)$, for OpD Bi-2223 single crystal. The data have been extracted and replotted from Ref. 38.

Table I. Annealing conditions and associated properties of two types of Bi-2223 single crystals used in this study.

Sample	Optimally doped (OpD)	Underdoped (UD)
Annealing condition	100% O_2, 500 °C	0.01% O_2, 600 °C
$T_{c\ onset}$	109 K	88.6 K
ρ_c at $T_{c\ onset}$	23.9 Ω·cm	148 Ω·cm
J_c at 35 K	216 A cm^{-2}	79.0 A cm^{-2}

The JPE devices were fabricated using photolithography and argon-ion milling. Figure 2(a) shows an optical microscope image of the Bi-2223 mesas. In this study, five mesas of different widths were fabricated on the same crystal base to investigate the mesa-size effect on the device characteristics. The mesas shown in Fig. 2(a) have varying widths of 25, 35, 45, 60, and 80 μm and labeled a, b, c, d, and e from left to right, respectively, with a common long edge length of 250 μm. The actual dimensions of each mesa were measured precisely using a stylus profiler. Figure 2(b) shows the cross-sectional profile of mesa d. The small protrusion at the top represents the profile of a 20-μm-wide silver electrode. The height of the mesa, which was measured to be 1.5 μm, indicates that it contains 830 IJJs. In Bi-2223, the thickness of a single IJJ is 1.8 nm, which is 1.2 times greater than that

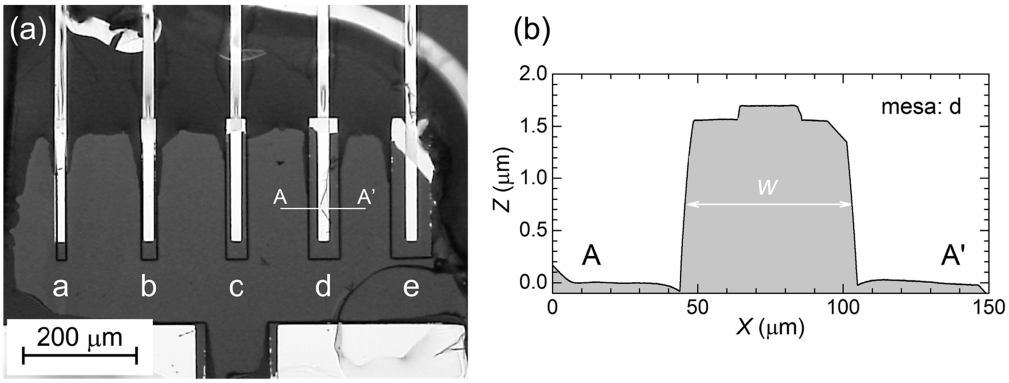

Fig. 2. (a) Optical microscope image of Bi-2223 IJJ mesas. The mesas have varying widths from left to right: 20, 35, 45, 60, and 80 μm and are labeled a–e, respectively; they all have a common long edge length of 250 μm. (b) Cross-sectional profile of mesa d measured using a stylus profiler. The small protrusion at the top of the mesa represents the profile of a 20-μm-wide silver electrode. The height of the mesa, 1.5 μm, corresponds to 830 IJJs.

of the IJJ in Bi-2212. Therefore, the junction density of the Bi-2223 phase is 83% lower than that of the Bi-2212 phase. This offers different etching rates for Bi-2223 and Bi-2212 phases.

The device structure employed in this study has been thoroughly addressed in numerous publications, providing a foundational basis for comparisons with prior research from different groups.[9–11)] This configuration notably offers scalability advantages, facilitating the concurrent production of multiple chips exhibiting consistent characteristics. As our study primarily revolves around transitioning the material from Bi-2212 to Bi-2223, the execution of systematic experiments utilizing multiple chips becomes imperative. However, the pursuit of enhanced device performance directs our attention to the necessity of refining the device configuration for improved cooling. This includes exploring optimal structures like the stand-alone type[13,40)] and gold-BSCCO-gold mesas.[41)] The emitting sample is mounted in a helium-flow cryostat, and terahertz emission is detected using a silicon-composite bolometer.

Figure 3 shows the temperature dependence of the *c*-axis electrical resistance (*R*–*T*) with black and red plots corresponding to the OpD and UD samples, respectively. In OpD, a drop in resistance due to the superconducting transition was observed at 101 and 109 K, whereas in UD, three superconducting transitions were observed at 65.7, 73.2, and 88.7 K. In parallel to the difference in T_c of OpD and UD crystals, the quasiparticle resistance shows a change depending on the excess oxygen. Specifically, the values of $R(T_{conset})/R(300\,K)$ were 1.7 (OpD) and 5.0 (UD). In the case of UD, the upturn in *R*–*T* is significant and consistent with the doping dependence investigated in previous studies.[33)]

The inset of Fig. 3 shows the *c*-axis current–voltage characteristics (IVCs) measured at bath temperature $T_b = 35$ K. Table I shows that J_c exhibited a 2.7-fold difference between OpD and UD. The maximum voltage in IVC was higher in UD with values of 0.58 V (OpD) and 1.76 V (UD), which is consistent with the *R*–*T* results. The back bending of the IVCs can be explained by the local temperature increase model due to Joule heating.[42,43)]

As shown in Fig. 1(b), magnetization measurements of Bi-2223 single crystals exhibit a single drop corresponding to the superconducting transition, confirming that the Bi-2223 phase constitutes nearly the entire sample volume. To more

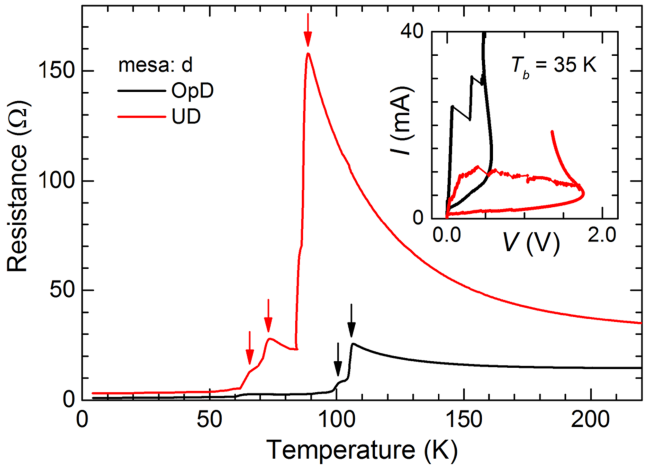

Fig. 3. Temperature dependence of the *c*-axis *R*–*T* for OpD and UD samples, represented by the black and red plots, respectively. The inset shows the *c*-axis IVCs measured at $T_b = 35$ K. Multiple transitions may suggest the presence of intergrowth layers; however, this was not the case. HRTEM imaging and magnetization measurements revealed that the volume fraction of the Bi-2223 phase was nearly 100% (see text).

precisely quantify the intergrowth layers within the crystal, the magnetic field should ideally be applied parallel to the *ab*-plane rather than along the *c*-axis. Nevertheless, as indicated by the HRTEM image in Fig. 1(a), the volume fraction of intergrowth layers is at most below 2%. This observation is consistent with the *c*-axis *R*–*T* data for the OpD sample shown in Fig. 3, which exhibits superconducting transitions only at 101 K and 109 K. Since both transitions occur above 100 K, they are attributed to the dominant Bi-2223 phase. In contrast, the UD sample—annealed from the same batch as the OpD crystal—shows no such transitions above 100 K. Instead, it exhibits transitions at 73.2 K and 88.7 K. Given that annealing at 600 °C is unlikely to induce a phase transformation from Bi-2223 to Bi-2212, these transitions are attributed to underdoped Bi-2223 phases with varying levels of excess oxygen δ.

Although Fig. 1(b) displays a single superconducting transition, the *R*–*T* characteristics of the mesa structure after microfabrication reveal multiple transitions. This suggests an inhomogeneous distribution of excess oxygen δ within the mesa, likely introduced during the fabrication process. The most plausible explanation is that thin contact mesas were unintentionally formed beneath the electrodes due to argon

ion over-etching, with the topmost contact mesa exhibiting a lower δ. The R–T results for the UD sample suggest that the mesa consists of approximately 3% ($T_c = 65.7$ K), 7% ($T_c = 73.2$ K), and 90% ($T_c = 88.7$ K) of Bi-2223 phases with varying degrees of underdoping.

Figure 4 illustrates the IVCs and bolometer output for mesa d of the UD sample at $T_b = 30$ K. The black arrows indicate the IVC generated by applying a single-cycle triangular wave. No features directly indicating the presence of an intergrowth phase were observed in the IVC. When the number of IJJs exceeds several hundred, multiple junctions transition to a finite voltage state simultaneously during bias sweeping. This makes it challenging to distinguish neighboring multi-branches. Even when we magnify the IVC shown in Fig. 4, we still observe irregularly spaced branches. Furthermore, at higher bias voltages, local Joule heating becomes significant, resulting in random and complex behavior of quasiparticle branches. However, a greater portion of the IJJs appeared to individually switch in the Bi-2223 system compared to Bi-2212. For example, the multiple branches observed around ±1.5 V in Fig. 4 have a fine structure that is distinct from conventional Bi-2212 JPEs.

Nonlinearly coupled IJJ systems have been reported to exhibit localized rotating modes arising from capacitive interactions between neighboring junctions.[44,45] Generally, imperfections in single crystals are expected to appear as non-uniform multiple-branch structures in the IVCs. However, in the case of Bi-2223, even an ideally perfect single crystal is anticipated to show irregularities in the IVCs due to weak capacitive coupling between IJJs. Although electromagnetic waves are generated in each Bi-2223 IJJ via the Josephson effect, phase synchronization among the stacked IJJs is difficult to achieve, likely leading to destructive interference of the emitted radiation. This mechanism will be discussed in greater detail in the following paragraph.

A spike-like behavior was observed in the bolometer output in the low-current region of the IVC return branch, as shown in Fig. 4. This indicated the emission of terahertz radiation from the Bi-2223 IJJ mesa. It is important to emphasize that this study presents the first instance of terahertz emission from Bi-2223 IJJs; the emission was not discernible from the OpD sample, but only from the UD sample, primarily because the maximum applied voltage in the OpD IVC was lower than that in the UD, as shown in the inset of Fig. 3. Specifically, the Josephson frequency in the OpD does not correspond to the cavity resonance condition determined by the mesa dimensions. Based on the bolometer sensitivity of 7×10^6 V W^{-1}, the detected emission power was estimated to be approximately 55 pW. Because the bolometer is positioned directly above the mesa in the c-axis direction and assuming a unidirectional radiation pattern in the transverse magnetic (TM) (1,0) mode, the integrated emission power can be calculated to be approximately 1 μW. If terahertz waves were emitted from intergrowth Bi-2212 IJJs in the Bi-2223 mesa, this emission power would be excessively high compared with those of earlier reports (e.g., see Ref. 18).

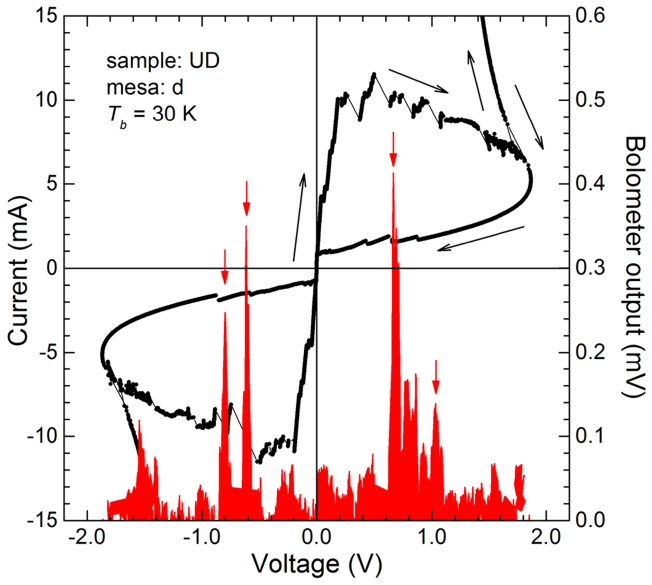

Fig. 4. Current–voltage characteristics (IVCs) and bolometer output for mesa d of the UD sample at $T_b = 30$ K. The black arrows in the figure points to the IVC generated by applying a single-cycle triangular wave. We observe a spike-like behavior in the low-current region in the bolometer output indicating terahertz emission (red arrows).

The single crystal used for JPE fabrication was cut from the same batch as the crystal used for magnetic susceptibility measurements [Fig. 1(b)]. The magnetic susceptibility indicates that the intergrowth Bi-2212 phase is less than 2% and it is dispersed without aggregation within the bulk crystal [Fig. 1(a)]. Therefore, it is reasonable to infer that the observed terahertz emission originates from the Bi-2223 IJJs rather than the intergrowth Bi-2212. Furthermore, previous studies suggest that synchronized IJJ-based terahertz emission requires a threshold number of approximately $N \sim 100$.[16]

A comparison of the integrated emission power between the Bi-2223 and B-2212 IJJs with the same number of IJJs revealed that the former produces a power output that is approximately one order of magnitude lower. In this study, weak emissions were observed from mesas c and d of the UD devices, with mesa c exhibiting an even lower output than mesa d. The experimental data for mesa c are not presented here due to its low signal-to-noise ratio. We fabricated over ten devices using Bi-2223 and comprehensively evaluated their characteristics. However, emission was detected only from two mesas on a single chip, as depicted in Fig. 2(a).

Adjacent IJJs were coupled using inductive and capacitive couplings, which are critical for macroscopic terahertz emission. The long-range interaction of the inductive coupling is expected to have a similar strength for Bi-2212 and Bi-2223. Consequently, the weak emission intensity observed in the Bi-2223 IJJs is believed to be an intrinsic characteristic resulting from their small capacitive coupling, which is inversely proportional to the thickness of the superconducting Cu-O layers.[44,46] Moreover, the presence of inner and outer planes with different T_c values in the Bi-2223 system has been suggested to result in a weaker capacitive coupling between adjacent IJJs. Previous studies have noted that differences in the probability of macroscopic quantum tunneling can explain the observed differences in the magnitude of capacitive coupling between Bi-2212 and Bi-2223.[47] Since the phase synchronization of the IJJs is essential for terahertz emission, it is natural to expect low emission power in the Bi-2223 phase, where the short-range capacitive coupling is small. Further verification of the

reproducibility and detection experiments using more sensitive detectors are necessary to clarify this point.

Figure 5 depicts the T_b dependence of the IVC and bolometer output for mesa d of the UD device. T_b is changed in 5 K increments from 20 to 50 K. In Fig. 5(a), the color of the symbols represents the bolometer output, as indicated by the color scale. In Fig. 5(b), an appropriate offset value is added to the vertical axis to improve visibility. This experiment demonstrates that terahertz emission occurs below 50 K, and larger bolometer output is obtained at a lower T_b. Complicated peak structures appear in the internal IVC branch region, reflecting the instability of the biased state. Although the effective temperature of the biased mesa was slightly higher than T_b, the thermal imaging experiments revealed that the temperature distribution in the low-bias region was almost uniform and nearly equal to T_b.[48] The diminishing radiation at $T_b > 50$ K is partly attributed to the IVC path aligning with the cavity resonance.

Since the detectable frequency bandwidth of the silicon-composite bolometer, equipped with a far-infrared (100 cm^{-1}) cut-on optical filter and a high-density polyethylene window, ranges from 0.15 THz to 3.0 THz, we confirmed that the characteristic frequency of the emitted electromagnetic waves lies within the terahertz range. However, the emission observed from the UD device was weak and fell below the sensitivity limit of the Fourier transform infrared spectrometer, hindering detailed analysis of the emission frequency. In the internal IVC branch region at low T_b, where a strong emission is obtained, accurate determination of the number of resistive IJJs is impeded by bias instability. Nevertheless, according to the Josephson relation, the emission frequency can be estimated from the bias conditions. As shown in Fig. 4, an intense emission is observed at $V = 1.03$ V in the outermost IVC branch, where all IJJs are resistive. By calculating the emission frequency using the Josephson relation with $N = 830$, we obtained $f_J = 0.59$ THz.

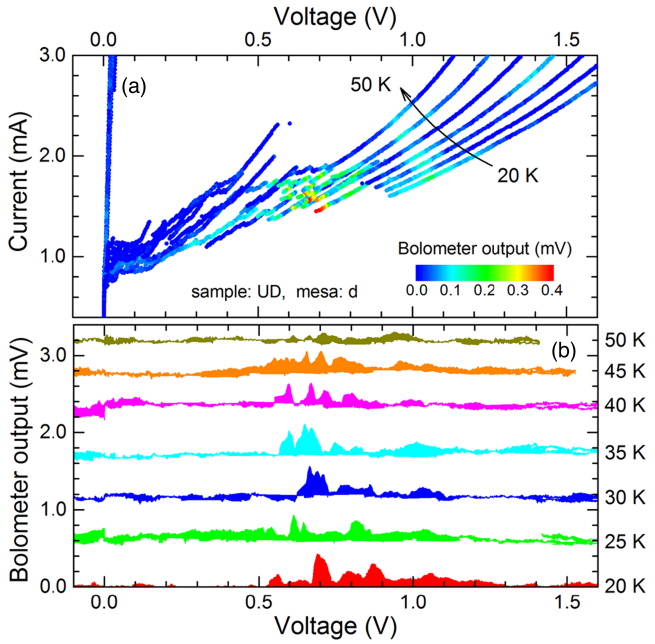

Fig. 5. (a) IVCs and (b) bolometer output for mesa d of the UD device, with bath temperature T_b. varied in 5 K increments from 20 to 50 K. In (a), the color of the symbols indicates the corresponding bolometer output, as shown on the color scale within the figure. In (b), an appropriate offset value was applied to the vertical axis to enhance visibility.

Assuming the excitation of the TM(1,0) mode, the refractive index n_r of Bi-2223 can be estimated to be 4.5.

Reducing the mesa size might increase the voltage per junction, thereby satisfying the emission conditions. However, adjusting the mesa size to meet the emission condition is not straightforward unless the refractive index n_r of Bi-2223 is known because it may also alter the cavity resonance frequency. To the best of our knowledge, there is no literature on the refractive index and dielectric constant of Bi-2223 in the terahertz range. Because these values represent a material property and determine the geometric cavity resonance condition, making them important for designing JPEs, a further discussion is necessary.

The mechanism of THz JPE, in which Josephson plasma is excited by self-oscillations and emitted into free space, is closely related to the coherent emission of surface plasmons observed in cuprate superconductors such as $La_{2-x}Ba_xCuO_4$[49] and $YBa_2Cu_3O_{6+x}$.[50] Although the link between charge order and the characteristics of JPEs remains unclear, it is notable that monochromatic continuous-wave emission occurs even without inversion symmetry breaking along the c-axis. Future time-domain spectroscopic studies of JPEs are expected to elucidate the coherence of Josephson self-oscillations and the dispersion of bulk plasmons. These insights may shed light on the origin of charge ordering in cuprates and the underlying mechanism of high-T_c superconductivity.

In summary, we reported the first observation of continuous terahertz emission from IJJs in Bi-2223 single crystals. We prepared two types of crystals, optimally doped and underdoped, and compared their electrical and terahertz emission characteristics. HRTEM imaging and magnetization measurements revealed that the volume fraction of the Bi-2223 phase was nearly 100%, and the multiple transitions observed in the R–T measurement could be explained by the presence of different Bi-2223 phases with varying levels of oxygen within the mesa. Weak, but detectable terahertz emissions were observed only in the underdoped device ($T_{conset} = 88.7$ K), whereas no radiation was observed in the optimally doped device ($T_{conset} = 109$ K). We presumed that the capacitive coupling between the Bi-2223 IJJs was weaker than that between the Bi-2212 IJJs, resulting in a low terahertz emission output. We estimated the emission frequency from the voltage values and obtained the effective refractive index of Bi-2223. Because Bi-2223 is a promising cuprate with T_c above 100 K, the observation of coherent terahertz emissions in this study is an important discovery that provides a new choice of materials for JPEs.

Acknowledgments The authors express their gratitude to Y. Nomura, H. Kambara, G. Kuwano, and R. Kobayashi for their valuable contributions to the extensive discussions. The design and development of the fabrication process for Bi-2223 JPEs were partly supported by the U. S. Department of Energy, Office of Science, Basic Energy Sciences, Materials Sciences and Engineering Division (UW, WKK). This study was supported by KAKENHI (Grants Nos. JP23681030, JP13J04811, JP25400349, JP26790032, JP26286006, JP19H02540, JP20K03849, and JP23K03317). This work was supported by JST, PRESTO under Grant No. JPMJPR24F5, Japan. The work at Hirosaki was supported by a Hirosaki University Grant for Distinguished Researchers from the fiscal year 2017 to 2018.

ORCID iDs Manabu Tsujimoto https://orcid.org/0000-0003-4296-5137
Asem Elarabi https://orcid.org/0000-0001-7541-3756
Yilmaz Simsek https://orcid.org/0000-0001-6166-1441
Wai-Kwong Kwok https://orcid.org/0000-0003-0030-084X
Shintaro Adachi https://orcid.org/0000-0002-5165-5088

Takao Watanabe https://orcid.org/0000-0002-9759-6976
Itsuhiro Kakeya https://orcid.org/0000-0003-4999-2111

1) S. S. Dhillon et al., J. Phys. D: Appl. Phys. **50**, 043001 (2017).
2) M. Tonouchi, Nat. Photonics **1**, 97 (2007).
3) B. Ferguson and X.-C. Zhang, Nat. Mater. **1**, 26 (2002).
4) B. S. Williams, Nat. Photonics **1**, 517 (2007).
5) S. Kumar, IEEE J. Sel. Top. Quantum Electron. **17**, 38 (2011).
6) A. Wade, G. Fedorov, D. Smirnov, S. Kumar, B. S. Williams, Q. Hu, and J. L. Reno, Nat. Photonics **3**, 41 (2008).
7) G. Scalari, C. Walther, M. Fischer, R. Terazzi, H. Beere, D. Ritchie, and J. Faist, Laser Photon. Rev. **3**, 45 (2009).
8) M. Asada and S. Suzuki, Sensors **21**, 1384 (2021).
9) L. Ozyuzer et al., Science **318**, 1291 (2007).
10) U. Welp, K. Kadowaki, and R. Kleiner, Nat. Photonics **7**, 702 (2013).
11) I. Kakeya and H. Wang, Supercond. Sci. Technol. **29**, 073001 (2016).
12) R. Kleiner, F. Steinmeyer, G. Kunkel, and P. Müller, Phys. Rev. Lett. **68**, 2394 (1992).
13) M. Tsujimoto et al., Phys. Rev. Lett. **108**, 107006 (2012).
14) T. Kashiwagi et al., Appl. Phys. Lett. **107**, 082601 (2015).
15) H. Sun et al., "Compact High-Tc Superconducting Terahertz Emitter with Tunable Frequency from 0.15 to 1 THz," Appl. Sci. **13**, 3469 (2023).
16) E. A. Borodianskyi and V. M. Krasnov, Nat. Commun. **8**, 1742 (2017).
17) M. M. Krasnov, N. D. Novikova, R. Cattaneo, A. A. Kalenyuk, and V. M. Krasnov, Beilstein J. Nanotechnol. **12**, 1392 (2021).
18) T. M. Benseman, K. E. Gray, A. E. Koshelev, W.-K. Kwok, U. Welp, H. Minami, K. Kadowaki, and T. Yamamoto, Appl. Phys. Lett. **103**, 022602 (2013).
19) M. Tsujimoto, S. Fujita, G. Kuwano, K. Maeda, A. Elarabi, J. Hawecker, J. Tignon, J. Mangeney, S. S. Dhillon, and I. Kakeya, Phys. Rev. Appl. **13**, 051001 (2020).
20) L. Y. Hao et al., Phys. Rev. Appl. **3**, 024006 (2015).
21) H. Minami, C. Watanabe, T. Kashiwagi, T. Yamamoto, K. Kadowaki, and R. A. Klemm, J. Phys. Condens. Matter **28**, 025701 (2016).
22) H. Sun et al., Phys. Rev. Appl. **10**, 024041 (2018).
23) K. J. Kihlstrom et al., Phys. Rev. Applied **19**, 034055 (2023).
24) M. Tsujimoto, K. Yamaki, K. Deguchi, T. Yamamoto, T. Kashiwagi, H. Minami, M. Tachiki, K. Kadowaki, and R. A. Klemm, Phys. Rev. Lett. **105**, 037005 (2010).
25) M. Tsujimoto, I. Kakeya, T. Kashiwagi, H. Minami, and K. Kadowaki, Opt. Express **24**, 4591 (2016).
26) T. Kashiwagi et al., J. Appl. Phys. **124**, 033901 (2018).
27) M. Tsujimoto, Y. Maeda, H. Kambara, A. Elarabi, Y. Yoshioka, Y. Nakagawa, Y. Wen, T. Doi, H. Saito, and I. Kakeya, Supercond. Sci. Technol. **28**, 105015 (2015).
28) H. Maeda, Y. Tanaka, M. Fukutomi, and T. Asano, Jpn. J. Appl. Phys. **27**, L209 (1988).
29) B. Liang, C. T. Lin, P. Shang, and G. Yang, Physica C **383**, 75 (2002).
30) E. Giannini, V. Garnier, R. Gladyshevskii, and R. Flükiger, Supercond. Sci. Technol. **17**, 220 (2004).
31) A. B. Kulakov, D. Maier, A. Maljuk, I. K. Bdikin, and C. T. Lin, J. Cryst. Growth **296**, 69 (2006).
32) K. Kadowaki, S. Yasunaga, and T. Yamamoto, Physica C **460–462**, 60 (2007).
33) T. Fujii, I. Terasaki, T. Watanabe, and A. Matsuda, Phys. Rev. B: Condens. Matter Mater. Phys. **66**, 024507 (2002).
34) S. A. Kivelson, Physica B Condens. Matter **318**, 61 (2002).
35) S. Okamoto and T. A. Maier, Phys. Rev. Lett. **101**, 156401 (2008).
36) S. Chakravarty, H.-Y. Kee, and K. Völker, Nature **428**, 53 (2004).
37) Z. Hao, C. Zou, X. Luo, Y. Ji, M. Xu, S. Ye, X. Zhou, C. Lin, and Y. Wang, Phys. Rev. Lett. **125**, 237005 (2020).
38) S. Adachi et al., Phys. Procedia **65**, 53 (2015).
39) T. Fujii, T. Watanabe, and A. Matsuda, J. Cryst. Growth **223**, 175 (2001).
40) T. Kitamura et al., Appl. Phys. Lett. **105**, 202603 (2014).
41) M. Ji et al., Appl. Phys. Lett. **105**, 122602 (2014).
42) C. Kurter, K. E. Gray, J. F. Zasadzinski, L. Ozyuzer, A. E. Koshelev, T. Yamamoto, K. Kadowaki, W.-K. Kwok, M. Tachiki, and U. Welp, IEEE Trans. Appl. Supercond. **19**, 428 (2009).
43) F. Rudau et al., Phys. Rev. B: Condens. Matter Mater. Phys. **91**, 104513 (2015).
44) M. Machida, T. Koyama, and M. Tachiki, Phys. Rev. Lett. **83**, 4618 (1999).
45) M. Machida and T. Koyama, Phys. Rev. B: Condens. Matter Mater. Phys. **70**, 024523 (2004).
46) T. Koyama and M. Tachiki, Phys. Rev. B: Condens. Matter **54**, 16183 (1996).
47) Y. Nomura, R. Okamoto, T.-A. Mizuno, S. Adachi, T. Watanabe, M. Suzuki, and I. Kakeya, Phys. Rev. B: Condens. Matter **100**, 144515 (2019).
48) M. Tsujimoto, H. Kambara, Y. Maeda, Y. Yoshioka, Y. Nakagawa, and I. Kakeya, Phys. Rev. Appl. **2**, 044016 (2014).
49) D. Nicoletti, M. Buzzi, M. Fechner, P. E. Dolgirev, M. H. Michael, J. B. Curtis, E. Demler, G. D. Gu, and A. Cavalleri, Proc. Natl. Acad. Sci. U. S. A. **119**, e2211670119 (2022).
50) D. Nicoletti et al., arXiv: 2504.02568.